Orfanidou *et al.*
Biotechnology for the Environment (2025) 2:6
https://doi.org/10.1186/s44314-025-00021-w

Biotechnology for the Environment

RESEARCH

Open Access

Engineering novel *Yarrowia lipolytica* whole-cell biocatalysts by cell surface display of the native Lip2 lipase for biodiesel production

Maria Orfanidou[1†], Eleftheria Panagiotidou[2,3†], Antonios M. Makris[1] and Eleni Theodosiou[1*]

Abstract

Yeast surface display (YSD) has proven to be a valuable tool in cellular engineering, particularly for conferring biocatalytic activities to cells, thereby enabling the creation of novel whole-cell biocatalysts. Compared to intracellular and secretion-based strategies, cell surface display of enzymes offers distinct advantages, including the elimination of enzyme recovery and purification steps, the resolution of substrate transport limitations, and enhanced activity, stability, and selectivity. In this work, YSD was employed to construct efficient display systems for *Yarrowia lipolytica* using the native lipase Lip2 fused with constitutive promoter-based anchoring vectors. The biocatalytic activity of the Lip2 biomass–bound recombinant strains was evaluated in transesterification reaction (butanolysis of p-nitrophenyl palmitate). The best-performing strain expressing the *LIP2* gene under the *UAS1B8-TMAL(250)* hybrid promoter was cultivated in a lab-scale bioreactor to identify crucial parameters that have to be fine-tuned for a scalable bioprocess that yields biomass of both high density and Lip2 activity. Harvested biomass was used to catalyze the synthesis of biodiesel (olive oil methanolysis) yielding under optimal reaction conditions 71.4% conversion after 48 h.

Keywords *Yarrowia lipolytica*, Hybrid promoter, Cell surface display, Lip2 lipase, Whole-cell biocatalyst, Biodiesel

Introduction

Immobilization of functional proteins or peptides on the membrane of microbial cells using cell surface display (CSD) technology is a valuable approach to endow them with unique cellular functions, ranging from novel catalytic activities and affinity binding for structure-based drug design to bioremediation and bio-monitoring properties [1].This "natural" immobilization is realized by fusing the genes that encode the protein/peptide of interest (POI) with an anchoring protein and subsequently expressing the fusion (N-terminal, C-terminal, or sandwich fusion) on the cell surface under the guidance of signal peptides [2, 3]. A CSD system includes three crucial structural components, namely the protein to be displayed, the carrier protein, and the microbial host. The characteristics of these components, as well as their interplay, greatly affect the display efficiency and the conformation of the protein and, ultimately, the functional properties of the POI [2, 4].

When designing novel whole-cell biocatalysts, CSD is a highly attractive approach since it affords protein immobilization along with precise control over gene expression, thus allowing for fine-tuning of protein synthesis and simplified processes of recovery, purification, and reuse [5]. CSD not only delivers renewable

†Maria Orfanidou and Eleftheria Panagiotidou contributed equally to this work.

*Correspondence:
Eleni Theodosiou
eleni.theodosiou@certh.gr
[1] Centre for Research and Technology Hellas, Institute of Applied Biosciences, Thermi, Thessaloniki 57001, Greece
[2] Department of Biology, School of Sciences and Engineering, University of Crete, Heraklion 70013, Greece
[3] Institute of Molecular Biology and Biotechnology, Foundation for Research and Technology-Hellas (FORTH), Heraklion 70013, Greece

self-immobilized biocatalysts but also overcomes various drawbacks of conventional immobilization methods, such as unwanted structural and functional alterations or even enzyme inactivation, low enzyme loading, dissociation, mass transfer limitations, and high costs of materials used [6]. Compared to expression of genes encoding enzymes that are secreted in the culture medium (free enzymes), CSD offers notable advantages. The displayed enzymes usually retain their functionality even under harsh reaction conditions, can be easily recovered after biomass harvesting via centrifugation or filtration (circumventing permeabilization, cell lysis, recovery from the medium), and multi-enzyme systems can be designed catalyzing cascade reactions or acting synergistically [7–10]. Finally, CSD of enzymes allows the host cells to readily access soluble substrates that cannot enter the cell due to their large molecular masses (e.g., cellulose, hemicellulose), while their intracellular enzymes transform the generated monomers (e.g., glucose) into valuable products, thus expanding the applications of engineered enzyme biocatalysts in industry. Such a case is the extracellular degradation of cellulose and the parallel uptake of the major product, glucose, for bioethanol production [5, 8].

CSD has been employed for the construction of whole-cell biocatalysts using various microbial cells, with yeasts being the most suitable hosts due to their safety (GRAS), relatively large cell size, rigid cell-wall structure, ease of genetic manipulation, standardized protocols for production of POI, and available cellular post translational processes (e.g., folding and glycosylation of heterologous expressed eukaryotic proteins) [3, 11]. CSD was first developed in *Saccharomyces cerevisiae* and later in *Pichia pastoris* [10, 12–20] and *Yarrowia lipolytica* [21–27]. One of the most crucial factors affecting the efficiency of the display is protein secretion and concomitantly the number of proteins displayed on the host [3, 11]. To achieve this, strategies aimed at enhancing protein secretion can be employed. These include the use of strong promoters [28], the design of synthetic promoters with upstream activating sequences (UASs) [28, 29], the selection of efficient signal peptides [30–32] and anchoring proteins [27, 31, 33, 34], the optimization of growth conditions [27–29], and host engineering to increase cell wall protein-carrying capacity or enhance secretory fluxes [35–38].

In this study, we used protein display technology to develop novel *Y. lipolytica* whole-cell biocatalysts suitable for the biodiesel industry, with potential applications beyond this. For that, we fused the native lipase *LIP2* gene, which encodes for an extracellular 1,3-regioselective lipase [39], with the native cell wall protein *YlPIR1* gene [21] and integrated the construct into the genome. In an effort to enhance *LIP2* expression levels, we evaluated the impact of native (*EXP1* and *H3*) and hybrid promoters (*UAS1B8-TMAL*) [28], multiple *LIP2* gene copies, and different genome integration sites (IntE_4 and IntF_3). Promoter strength was quantified using flow cytometry by measuring the fluorescence emitted by the YlPir1-mCherry reporter fusion protein, while successful Lip2 membrane anchoring was confirmed by confocal microscopy using YlPir1-mCherry (membrane bound) in combination with the EGFP green fluorescent protein (cytosolic). The newly constructed strains were physiologically characterized, and the catalytic activity of their biomass was evaluated for the butanolysis of p-nitrophenyl palmitate (pNPP) in hexane. The strain with the highest activity was selected for scale-up cultivation in a 3-L benchtop bioreactor, where key parameters influencing both biomass production and biomass-bound Lip2 activity were identified. The harvested biomass was subsequently utilized to catalyze the methanolysis of olive oil for biodiesel production, and critical reaction conditions were optimized.

Materials and methods

Strains and culture conditions

Escherichia coli Mach1™-T1 (Thermo Fisher Scientific, MA, USA) was used for TA cloning. NEB® 5-alpha Competent *E. coli* (New England Biolabs, MA, USA) was used for shuttle vector propagation. Cells were grown in 5-mL Luria–Bertani (LB) medium supplemented with 100 μg/mL kanamycin or ampicillin for Mach1™-T1 and NEB® 5-alpha *E. coli* cells, respectively. For LB agar plates, 15 g/L agar was added prior to sterilization. Bacterial cultures were incubated at 37 °C and 150 rpm.

Wild-type *Y. lipolytica* MUCL 28849 (BCCM/MUCL, Brussels, Belgium) was transformed with site-specific integrative vectors using the lithium acetate (LiAc) method [40]. *Y. lipolytica* transformants were inoculated into 5-mL YPG medium and grown overnight at 30 °C and 150 rpm. The precultures were used to inoculate 25-mL YPG medium in 100-mL shaking flasks with an initial OD_{600nm} of 0.25. Main cultures were incubated for 96 h at 30 °C and 150 rpm. Wild-type *Y. lipolytica* MUCL 28849 strain was used as control. YPG medium contained 10 g/L yeast extract, 20 g/L peptone, and 20 mL/L glycerol (PENTA Chemicals Unlimited, Prague, Czech Republic). YPG medium was supplemented with 5% v/v olive oil, waste olive oil, or molasses to test their suitability as extra carbon source. In all cases (i.e., flask or bioreactor setup), the growth rate of the recombinant strains was monitored by determining the OD_{600nm} using a UV/

Vis spectrophotometer (BioPhotometer, Eppendorf, Germany).

Construction of vectors

General cloning was performed according to Georgiadis et al. [28]. Using the genomic DNA (gDNA) of *Y. lipolytica* MUCL 28849, the open reading frame (ORF) without stop codon of *YlPIR1* gene was amplified (GenBank accession number: AF336989) using the primers YlPIR1-BamHI-F and YlPIR1-EcoRI-nS-R. Recombinant plasmid pCRII-*LIP2* was used as template for PCR amplification of *LIP2* gene using the primers LIP2-EcoRI-F and LIP2-SalI-R. Plasmid pLentiCRISPRv2-*mCherry* was a gift from Agata Smogorzewska (RRID:Addgene_99154) and served as template for PCR amplification of the *mCherry* gene using the primers mChe-B-E and mChe-XhoI. *EGFP* gene was PCR amplified using plasmid pcDNA3-*EGFP* (RRID:Addgene_13031) as template and the primers mChe-B-E and mChe-XhoI.

For genomic integration, the plasmids pYL*EXP1* IntE_4, pYL*EXP1* IntF_3, pYL*H3* IntF_3, and pYL*UAS1B8-TMAL(250)* IntC_2 bearing the *YlPIR1-LIP2* fusion were used [28]. The sites of integration were 4, 3, and 2 in the chromosomes E (IntE_4), F (IntF_3), and C (IntC_2), respectively. Using the restriction enzymes BamHI and EcoRI, *YlPIR1* was subcloned downstream of *EXP1* promoter, and recombinant plasmid pYL*EXP1-YlPIR1* IntE_4 was generated. Plasmid pCRII-TOPO-*LIP2* and pYL*EXP1-YlPIR1* IntE_4 were digested with EcoRI and SalI and ligated to construct the pYL*EXP1-YlPIR1-LIP2* IntE_4 vector. Plasmid pYL*EXP1-YlPIR1-LIP2* IntF_3 was constructed after digestion of pYL*EXP1* IntF_3 with BamHI and XhoI and pYL*EXP1-YlPIR1-LIP2* IntE_4 with BamHI and SalI and ligated. Fused genes *YlPIR1-LIP2* and plasmid pYL*H3* IntF_3 were ligated using BamHI and SalI restriction enzymes for generating vector pYL*H3-YlPIR1-LIP2* IntF_3. For C_2 integrative vector bearing the hybrid promoter, *UAS1B8-TMAL(250)* was amplified with PCR from pYL*UAS1B8-TMAL(250)* IntC_2 [28] using the pCfB-F and pCfB-R primers (primers for Gibson transfer of existing promoters into other *Yarrowia* integrative vectors) and then Gibson assembled into pCfB4782 (RRID: Addgene_106141) [41]. Plasmid pBluescript SK(−) and *YlPIR1* were ligated using BamHI and SalI restriction enzymes. Then *LIP2* was subcloned into pBlue-*YlPIR1* after digestion with EcoRI and SalI. Plasmid pBlue-*YlPIR1* was digested with BamHI and XhoI, while pYL*UAS1B8_TMAL(250)* IntC_2 was digested with BglII and SalI resulting in vector pYL*UAS1B8-TMAL(250)-YlPIR1-LIP2* IntC_2.

For integrative vectors bearing the fusion *YlPIR1-mCherry*, vectors pYL*EXP1-YlPIR1* IntE_4, pYL*EXP1* IntF_3, pYL*H3* IntF_3, and pYL*UAS1B8_TMAL(250)* IntC_2 were used. Plasmid pCRII-TOPO-*mCherry* was digested with EcoRI and XhoI and ligated with pYL*EXP1-YlPIR1* IntE_4 for generating vector pYL-*EXP1-YlPIR1-mCherry* IntE_4. *MCherry* was subcloned downstream of pEXP1 using BamHI and XhoI restriction enzymes, and vector pYL*EXP1-mCherry* IntF_3 was generated. Then plasmids pYL*EXP1-mCherry* IntF_3 and pCRII-TOPO-*YlPIR1* were digested with BamHI and EcoRI and ligated. The fusion *YlPIR1-mCherry* was amplified with PCR and Gibson-assembled into pYL*H3* IntF_3 to generate vector pYL*H3-YlPIR1-mCherry* IntF_3. *MCherry* was subcloned into pBlue-*YlPIR1* using EcoRI and XhoI restriction enzymes. Plasmid pBlue-*YlPIR1-mCherry* was then digested with BamHI and XhoI, while pYL*UAS1B8_TMAL(250)* IntC_2 was digested with BglII and SalI. After ligation, vector pYL*UAS1B8-TMAL(250)-YlPIR1-mCherry* IntC_2 was generated. Finally, for the construction of the integrative vector bearing the *EGFP* gene for cytoplasmic expression, the plasmids pCRII-TOPO-*EGFP* and pYL*H3* IntF_3 were ligated using BamHI and XhoI restriction enzymes resulting in vector pYL*H3-EGFP* IntF_3. All plasmids and primers used are listed in Supplementary Tables S1and S2, respectively.

Yeast transformation

For the selection of transformants bearing one copy of the desirable cassette, the gene *NAT* (encoding for nourseothricin N-acetyl transferase), conferring resistance to the antibiotic nourseothricin, was used as selectable marker. To enable the selection of the second copy of the cassettes, Cre-mediated excision of the *NAT* gene through LoxP regions was performed, using the episomal vector pHYL*H3-Cre rec*. Primers used for verification of successful excision of *NAT* are listed in Supplementary Table S3. Strains EXP1-YlPIR1-LIP2 IntE_4 and EXP1-YlPIR1-mCherry IntE_4 were transformed with the pHYL*H3-Cre rec* episomal vector using the LiAc method [40]. Strain EXP1-YlPIR1-LIP2 IntE_4 was then transformed with the plasmids pYL*EXP1-YlPIR1-LIP2* IntF_3 and pYL*H3-YlPIR1-LIP2* IntF_3 for the development of strains with two *LIP2* copies, i.e., EXP1-YlPIR1-LIP2 IntE_4/EXP1-YlPIR1-LIP2IntF_3 and EXP1-YlPIR1-LIP2 IntE_4/H3-YlPIR1-LIP2 IntF_3, respectively. Strain EXP1-YlPIR1-mCherry IntE_4 was transformed with the plasmids pYL*EXP1-YlPIR1-mCherry* IntF_3, pYL*H3-YlPIR1-mCherry* IntF_3, and pYL*H3-EGFP* IntF_3 for the development of three new strains, i.e., EXP1-YlPIR1-mCherry IntE_4/EXP1-YlPIR1-mCherry IntF_3, EXP1-YlPIR1-mCherry IntE_4/H3-YlPIR1-mCherry IntF_3, and EXP1-YlPIR1-mCherry IntE_4/H3-EGFP IntF_3,

respectively. Excision of the *NAT* gene using the plasmid pHYL*H3-Cre rec* was also performed in the new strains using the LiAc protocol [40].

Flow cytometry analysis and fluorescence microscopy observation

Yeast transformants were incubated for 96 h (YPG, initial OD_{600nm} 0.25, 30 °C, 150 rpm), and 200 µL from each culture was collected every 24 h. Prior to flow cytometry analysis, cells were washed two times with phosphate-buffered saline (PBS) pH 7.4 (13,500 × g for 2 min) and diluted (20-µL cells in 980-µL PBS). The analysis was performed using BriCyte E6 flow cytometer (Mindray Bio-Medical Electronics, Nanshan, China). Data were analyzed using FlowJo™ v10 Software (BD Life Sciences, Franklin Lakes, NJ, USA) according to Georgiadis et al. [28]. The geometric mean of the generated data was used to calculate the fluorescence intensity of each sample, while the number of events recorded was set to 50,000. For confocal microscopy, cells were centrifuged at 13,500 × g for 2 min, washed two times with PBS, and resuspended in PBS (50-µL cells in 100-µL PBS) before being examined under confocal laser scanning microscope LSM780 (Carl Zeiss, Jena, Germany), following Zeiss software instructions. Images for mCherry fluorescent protein were taken at 543 nm while for EGFP at 488 nm.

Enzymatic activity assays

Tributyrin-agar plate assay

For the qualitative screening of the lipolytic activity of the recombinant strains, a tributyrin agar-based assay was performed (modified [42]). For that, both wild-type and recombinant yeast cells were tested using two-layer plates, containing an upper tributyrin agar layer (2% v/v liquid tributyrin, 20 g/L tributyrin agar) (Merck KGaA, Darmstadt, Germany) and a lower stabilizing agarose layer (2% w/v agarose) (Life Technologies, Carlsbad, CA, USA). The upper tributyrin agar layer was perforated using sterile pipette tips to form 6-mm wells. In each well, liquid culture or supernatant (after centrifugation) was transferred, containing cell surface-displayed lipase or secreted extracellular lipases, respectively. In the first case, appropriate volume of each culture was transferred to each well so that the number of cells (based on OD_{600nm}) was equal in all samples ($OD_{lowest} \times 100\ \mu L = OD_{culture} \times V_{culture}$). For the supernatants, 1 mL of a 72-h culture was centrifuged for 5 min at 14,000 rpm, and 100 µL of the supernatant was transferred to each well. The agar plates with culture samples and supernatants were incubated at 30 °C or stored in the refrigerator at 4 °C, respectively, and the clear halo formed around the colonies was monitored.

pNPP assay

To determine the transesterification activity of *Y. lipolytica* cells harboring the Lip2 display systems, a spectrophotometric method was performed, based on monitoring the released p-nitrophenol (pNP) during the transesterification of p-nitrophenyl palmitate (pNPP) (Thermo Fisher GmbH, Kandel, Germany) with butanol (modified [43]). For that, *Y. lipolytica* recombinant strains were used to inoculate overnight YPG precultures (5 mL, 30 °C, and 150 rpm). These precultures were then used to inoculate 25-mL YPG in 100-mL shake flasks at an initial OD_{600nm} 0.25 that served as the assay cultures. Cells were grown for 72 h at 30 °C and 150 rpm shaking. The cells were harvested by centrifugation (10 min at 4000 rpm) from a 72-h assay culture (stationary phase), washed twice with ddH_2O, and lyophilized for 24 h (Freeze Dryer LyoQuest, Telstar, Barcelona, Spain). The transesterification mixture consisted of 5-mg lyophilized whole-cell biocatalyst, 0.5-mL pNPP solution (20 mmol/L n-hexane), and 0.5-mL butanol (2 mol/L n-hexane). The reaction was carried out in 2-mL glass vials, at 40 °C and 400 rpm, for 5 h. At time 0 and every 1 h, 10 µL of the reaction mixture was transferred to 990 µL of absolute ethanol to terminate the reaction, and pNP was detected at 310 nm using a UV–Vis spectrophotometer (UV-2600 Spectrophotometer, Shimadzu Europa GmbH, Duisburg, Germany). The lipase Lipozyme® RM (Novozymes A/S, Bagsværd, Denmark) was used as positive control.

Biocatalyst production in a 3-L benchtop bioreactor

To investigate crucial parameters for biocatalytic biomass production, the strain with the best catalytic performance (i.e., UAS1B8-TMAL(250)-YlPIR1-LIP2 IntC_2) was employed. For that, a 3-L benchtop bioreactor (Minifors 2, Infors HT, Bottmingen, Basel, Switzerland) was filled with 1-L YPG medium and inoculated at an initial OD_{600nm} of ~ 0.5 using an overnight 100-mL preculture (28 °C, 150 rpm). The pO_2 was set at 40% and maintained at this level by controlling the agitation speed (150–300 or 500–800 rpm) and the air gassing rate (1–1.5 vvm). The temperature was controlled during the process (28 °C) while the pH not (initial pH ~ 6.8). To avoid excessive foaming, Antifoam C Emulsion (Merck KGaA, Darmstadt, Germany) diluted in water (10% active silicone) was added. Samples were withdrawn at regular intervals to monitor growth (OD_{600nm}), glycerol uptake rate, and biocatalyst performance using the transesterification assay (*see pNPP assay*). Glycerol was determined

using an UltiMate 3000 HPLC System equipped with a RefractoMax 521 Refractive Index Detector (Thermo Fisher Scientific Inc., Waltham, MA, USA) and a Hi-Plex column (250×4.6 mm PN: PL1570-6830, Agilent Technologies, Santa Clara, CA, USA). Both detector and column temperature were set at 40 °C. For the elution, 14-mM H_2SO_4(aq) was used at a flow rate 0.2 mL/min.

Enzymatic biodiesel production using Y. lipolytica whole cells

For the enzymatic production of biodiesel, transesterification of olive oil with methanol was carried out at 40 °C (200 rpm), and samples were withdrawn for GC analysis. The molar ratio of methanol to olive oil (3:1) and biocatalyst loading (20% w/w_{oil}) were kept constant, while water content, stepwise alcohol addition, and silica gel in the reaction mixture were studied for their impact on the methanolysis of olive oil. Biocatalyst reusability was also evaluated. Gas chromatography was performed with a Shimadzu QP2010 Ultra gas chromatograph (Shimadzu Europa GmbH, Duisburg, Germany) equipped with a hydrogen flame ionization detector and SP®−2340 Capillary GC Column (600 m×0.25 mm×0.20 um; Supelco, Bellefonte, PA, USA). The injector and detector temperatures were set at 250 °C. The column temperature was held at 100 °C for 5 min, then raised to 240 °C at a rate of 4.0 °C/min, and maintained for 30 min. The carrier gas used for the analysis was helium at a flow rate of 20 cm^3/min. The GCMSsolution software was used for data processing. Methyl heptadecanoate (C17:0, 99% purity, Sigma-Aldrich, St. Louis, USA) diluted in n-hexane (10 mg/mL) was used as internal standard in order to quantify the composition of fatty acid methyl esters (FAMEs). The FAMEs content present in the reaction mixture was calculated based on the peak area ratios of the corresponding FAMEs and internal standard peak areas (C17:0 ME) according to the EN 14103 standard method [44] and expressed as a mass fraction in percent.

$$FAME = \frac{(\Sigma A - AI)}{AI} \times \frac{(CI \cdot VI)}{msample} \times 100\%$$

where, ΣA: total peak area from the FAME C14:0 to C24:1, AI: peak area of methyl heptadecanoate, CI: concentration in milligram per milliliter of the methyl heptadecanoate solution, VI: volume in milliliter of the methyl heptadecanoate solution, and m: mass in milligram of the sample.

Results and discussion

Construction of Lip2 surface display systems for *Y. lipolytica*

It is well documented that promoters regulate gene expression at various levels by controlling the direction and intensity of transcription and thus are critical factors that dictate both secretion and activity of the target enzyme [45]. For surface display systems, both constitutive and inducible promoters can be used [46, 47]. In addition, apart from endogenous promoters, synthetic or hybrid promoters can be constructed via promoter engineering to further improve expression levels [28, 48, 49]. In *Y. lipolytica,* the constitutive native *TEF1* and the inducible hybrid *hp4d* promoter are the most commonly used for heterologous gene expression. Herein, in order to display the Lip2 lipase on the yeast cell surface, the *YlPIR1* gene (858 bp without the stop codon) encoding the cell wall protein YlPir1 was fused with the *LIP2* gene (1002 bp), and the constructed recombinant integrative pYL*Prom-YlPIR1-LIP2* expression cassette was used to transform *Y. lipolytica* cells [21]. To analyze and optimize the cell surface display of Lip2, various plasmids with

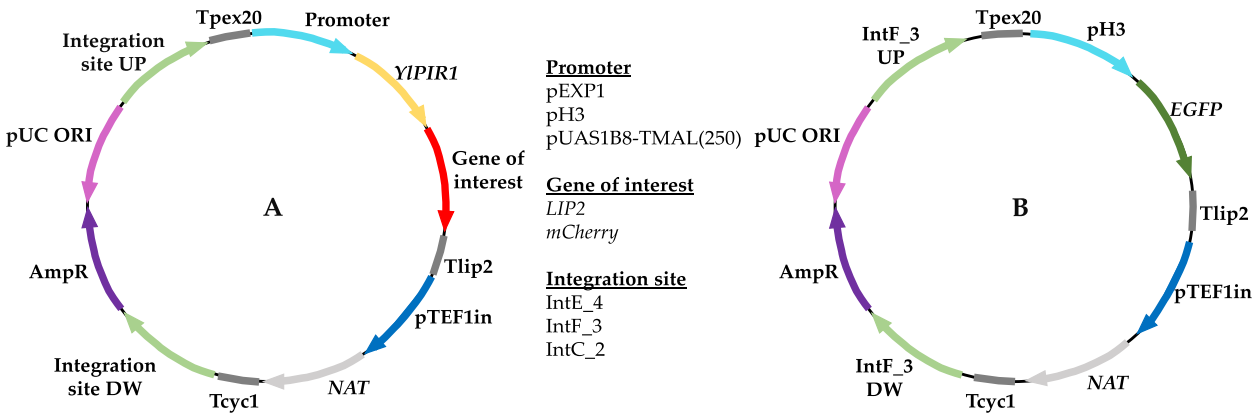

Fig. 1 Maps of the integrative expression cassettes for the Lip2 surface display systems for *Y. lipolytica* constructed in this study. **A** General map of the integrative pYL vector constructed for the expression of genes of interest on cell surface. **B** Map of integrative pYL*H3-EGFP* IntF_3 for the expression of *EGFP* gene and the localization of the protein in the cytoplasm of yeast cells. Expression cassettes were confirmed by double restriction enzyme digestion and Sanger sequencing

verified suitability in previous studies [31] were designed (Fig. 1). The expression cassettes were integrated into the genome, while the *NAT* resistance gene was used as marker for selection on YPD-NAT and YPG-NAT plates.

Since the expression levels of the *LIP2* gene are regulated by promoter strength, three promoters, two native (*EXP1*, *H3*) and one hybrid (*UAS1B8-TMAL(250)*), were tested, along with their respective genomic integration site (IntE_4, IntF_3, IntC_2). Additionally, multiple copies of the *LIP2* gene were inserted to evaluate whether the activity of the whole-cell biocatalyst could be enhanced. To analyze the effects of promoter type, integration site, and number of *LIP2* gene copy number on yeast physiology and Lip2 activity, various display systems were constructed, as summarized in Table 1, and used to generate recombinant *Y. lipolytica* cells.

Evaluation of surface display systems using reporter genes driven by native and hybrid promoters

The fluorescence activity of cells from the newly constructed recombinant strains was evaluated every 24 h, enabling quantification of *mCherry* reporter gene expression across the entire transfected population. In all cases, activity was steadily increasing until it culminated at the stationary phase (96-h cultures) (Fig. 2). When a single *mCherry* copy was integrated, it was found that neither the integration locus (IntE_4 or IntF_3) nor the type of the native promoter (*EXP1* or *H3*) had any significant impact on the fluorescence activity, which remained low at all-time points, only slightly exceeding the autofluorescence of wild-type cells. Similarly, the dual system incorporating two gene copies under the control of pEXP1 and pH3 resulted in low *mCherry* expression levels. Interestingly, when the dual system under the pEXP1 was used, the generated strain stood out from the very beginning (24 h) and kept its high fluorescence activity until the end of cultivation that was 1.6, 2.1, 2.0, and 2.0-fold higher compared to the control, at each sampling time point, respectively. On the other hand, cells containing a single *mCherry* copy under the hybrid promoter (*UAS1B8-TMAL(250)*) similarly exhibited high fluorescence, but this was observed only after 72 h of cultivation, however, at levels comparable to the strain bearing two gene copies under the strength of the pEXP1: 1.6 and 1.7-fold higher than the control at 72 and 96 h of cultivation.

The highest activities of the hybrid and the double *EXP1* native promoters were confirmed through confocal laser scanning microscopy (CLSM) that was employed not only to assess fluorescence intensity but also to verify successful anchoring on the cell surface and determine protein localization. The analysis employed the constitutively red fluorescent YlPir1-mCherry fusion protein (membrane protein) and the green fluorescent protein EGFP (cytoplasmic protein) as counterstains. Yeast cells expressing *mCherry* were successfully imaged (Fig. 3B, C, D, E, F, G, H), whereas the control strain *Y. lipolytica*

Table 1 List of the constructed Lip2 surface display systems and the generated novel recombinant *Y. lipolytica* strains in this study

pYL constructs	Promoter	Int. site	Gene
Native promoters with one gene copy			
EXP1-YlPIR1-mCherry IntE_4	*EXP1*	IntE_4	*mCherry*
EXP1-YlPIR1-mCherry IntF_3	*EXP1*	IntF_3	*mCherry*
H3-YlPIR1-mCherry IntF_3	*H3*	IntF_3	*mCherry*
EXP1-YlPIR1-LIP2 IntE_4	*EXP1*	IntE_4	*LIP2*
EXP1-YlPIR1-LIP2 IntF_3	*EXP1*	IntF_3	*LIP2*
H3-YlPIR1-LIP2 IntF_3	*H3*	IntF_3	*LIP2*
Native promoters with two gene copies			
EXP1-YlPIR1-mCherry IntE_4/EXP1-YlPIR1-mCherry IntF_3	*EXP1* *EXP1*	IntE_4 IntF_3	*mCherry* *mCherry*
EXP1-YlPIR1-mCherry IntE_4/H3-YlPIR1-mCherry IntF_3	*EXP1* *H3*	IntE_4 IntF_3	*mCherry* *mCherry*
EXP1-YlPIR1-mCherry IntE_4/H3-EGFP IntF_3	*EXP1* *H3*	IntE_4 IntF_3	*mCherry* *EGFP*
EXP1-YlPIR1-LIP2 IntE_4/EXP1-YlPIR1-LIP2 IntF_3	*EXP1* *EXP1*	IntE_4 IntF_3	*LIP2* *LIP2*
EXP1-YlPIR1-LIP2 IntE_4/H3-YlPIR1-LIP2 IntF_3	*EXP1* *H3*	IntE_4 IntF_3	*LIP2* *LIP2*
Hybrid promoters with one gene copy			
UAS1B8-TMAL(250)-YlPIR1-mCherry IntC_2	*UAS1B8-TMAL(250)*	IntC_2	*mCherry*
UAS1B8-TMAL(250)-YlPIR1-LIP2 IntC_2	*UAS1B8-TMAL(250)*	IntC_2	*LIP2*

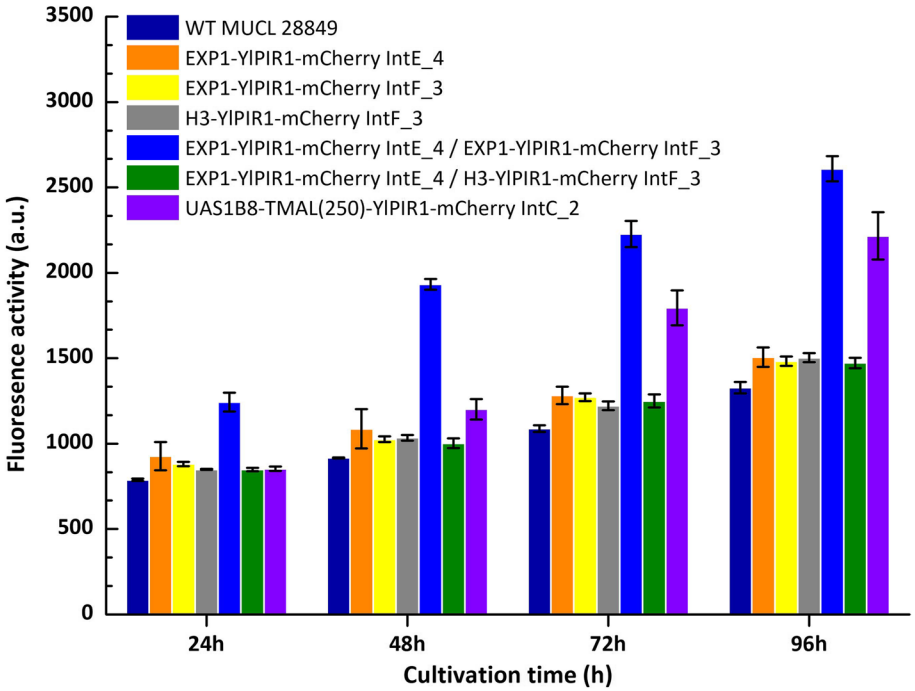

Fig. 2 Effect of promoters on display efficiencies. The activity of promoters as determined by flow cytometry and presented as fluorescence activity of the reporter mCherry protein after cultivation of recombinant *Y. lipolytica* strains in YPG medium for 96 h (30 °C, 150 rpm). Sample was taken every 24 h. Fluorescence activity is given as mean value in a.u. from three biological replicates ($n = 3$) with standard deviations shown as error bars

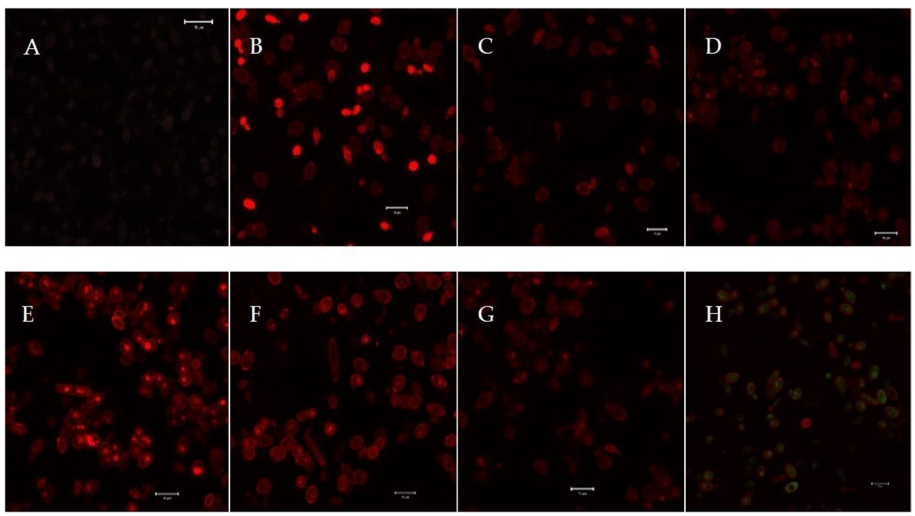

Fig. 3 Fluorescence images obtained using confocal laser scanning microscopy (CLSM). CLSM allowed the simultaneous detection of fluorescent cells and the localization of the membrane mCherry and the cytoplasmic EGFP protein of **A** wild-type *Y. lipolytica* MUCL 28849 as control, **B** EXP1-YlPIR1-mCherry IntE_4, **C** EXP1-YlPIR1-mCherry IntF_3, **D** H3-YlPIR1-mCherry IntF_3, **E** UAS1B8-TMAL(250)-YlPIR1-mCherry IntC_2, **F** EXP1-YlPIR1-LIP2 IntE_4/EXP1-YlPIR1-LIP2 IntF_3, **G** EXP1-YlPIR1-LIP2 IntE_4/H3-YlPIR1-LIP2 IntF_3, and **H** EXP1-YlPIR1-mCherry IntE_4/H3-EGFP IntF_3 after 72-h cultivation in YPG at 30 °C and 150 rpm

MUCL 28849 exhibited negligible fluorescence (Fig. 3A). Furthermore, when a dual reporter-gene system combining *mCherry* and *EGFP* was utilized, with both reporter fluorophores co-transfected into *Yarrowia* cells, the cell wall localization of YlPir1-mCherry became more pronounced (Fig. 3H). These findings demonstrate that

all six designed plasmids (Table 1) are suitable for protein display. However, strains carrying a single *mCherry* copy under the *UAS1B8-TMAL(250)* hybrid promoter and those with a double *mCherry* copy under the *EXP1* native promoter exhibited the highest fluorescence levels (Fig. 2E and F).

Growth and enzymatic activity of the engineered strains

To evaluate the effect of the display systems on the growth of the recombinant strains, cells were cultivated in YPG medium, and samples were withdrawn at regular intervals to determine the growth rate (h^{-1}). Figure 4A shows the time course of the cultivations of Lip2-displaying *Y. lipolytica* strains harboring the constructed integration cassettes. As seen in Fig. 4A, in all cases, neither the type of promoter nor the number of *LIP2* gene copies negatively impacted the growth rate of the recombinant strains. All strains exhibited similar growth rates, ranging from 0.34 to 0.36 h^{-1}; however, the strain containing the hybrid promoter produced the lowest biomass among all tested strains, hinting towards a heavier metabolic burden imposed on strain under this condition.

To quantify the activity of the Lip2 catalytic biomass, an enzymatic protocol based on the transesterification of pNPP with butanol was used [43]. The butanolysis of pNPP releases p-nitrophenol (pNP) that absorbs at 310 nm and can be determined spectrophotometrically. In this study, the release of the pNP was monitored over a 5-h period using lyophilized biomass as the catalyst, with the activity expressed in μmoles pNP per gram lyophilized biomass. The performance of the novel biocatalysts was also compared to the commercially available Lipozyme® RM lipase (Fig. 4B), which exhibited the highest transesterification activity, reaching a maximum (1515 ± 40 $\mu moles_{pNP}/g_{biocatalyst}$) within the first hour of reaction. The highest activity was determined using the strain bearing one *LIP2* copy under the hybrid promoter, i.e., UAS1B8-TMAL(250)-YlPIR1-LIP2 IntC_2; however, it did not exceed that of Lipozyme® RM lipase that was 2.5-fold higher. The lower activity of the cell surface-displayed Lip2 compared to the commercially available immobilized lipase may be attributed to enzyme detachment or denaturation, cell membrane degradation, or the impact of reaction conditions on cell integrity. Immobilization typically involves cross-linking or binding the enzyme to a solid matrix, which provides a more rigid structure, offering resistance to destabilizing effects. In contrast, the lack of such a protective matrix renders cell surface-displayed enzymes more vulnerable to operational challenges (e.g., agitation, organic solvent). Considering these factors, the whole-cell biocatalyst performed significantly well compared to the commercially available Lipozyme RM. Both dual systems, EXP1-YlPIR1-LIP2 IntE_4/EXP1-YlPIR1-LIP2 IntF_3 and EXP1-YlPIR1-LIP2 IntE_4/H3-YlPIR1-LIP2 IntF_3, exhibited high activities that were comparable to that of EXP1-YlPIR1-LIP2 IntF_3. When only one gene copy was used, the strain EXP1-YlPIR1-LIP2 IntF_3 demonstrated higher Lip2 activity than EXP1-YlPIR1-LIP2 IntE_4, suggesting that the IntF_3 genomic integration site is more favorable for *LIP2* expression. Regardless of the integration site, pEXP1 resulted in higher activities compared to the pH3. Although *EXP1* IntE_4 and *H3* IntF_3 promoters were

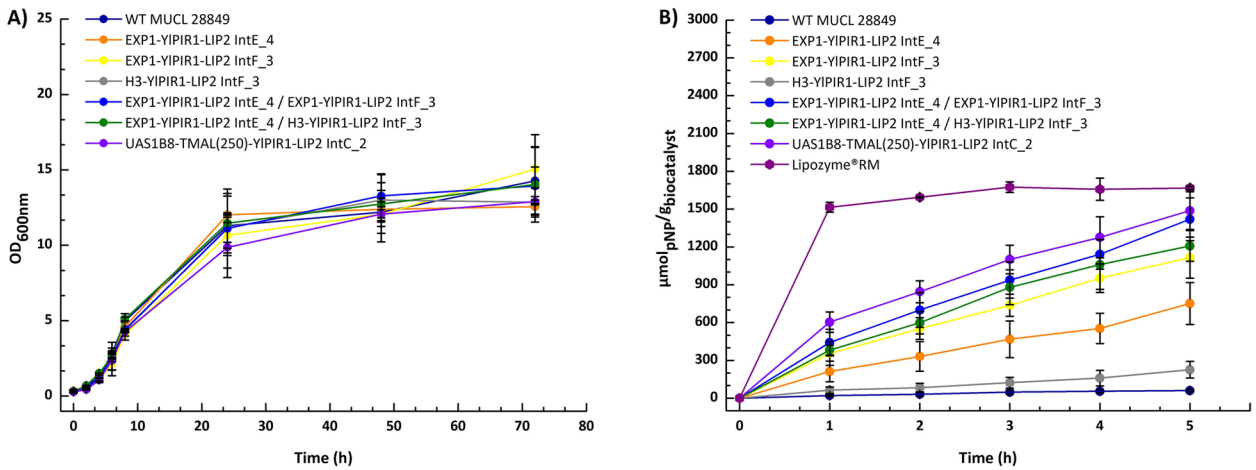

Fig. 4 Effect of Lip2 display systems on the growth of recombinant strains and the transesterification activity of their lyophilized biomass. **A** Growth profile (OD_{600nm}) of recombinant *Y. lipolytica* strains carrying the *YlPIR1-LIP2* expression cassetes cultured in YPG medium at 30 °C and 150 rpm. **B** Transesterification activity, measured photometrically at 310 nm using the pNPP assay, was expressed as μmoles pNP produced per gram of biocatalyst, i.e., either lyophilized biocatalytic biomass or immobilized enzyme. Lipozyme® RM lipase served as the positive control. Data points represent the mean values of at least three biological replicates ($n \geq 3$), with standard deviations shown as error bars

found to be the weakest ones when used solely, they displayed a synergistic effect when combined.

To rapidly screen and evaluate the efficiency of Lip2-displayed systems, a tributyrin agar-based method was employed and compared to the quantitative results obtained above. This method relies on the formation of a halo around colonies growing on tributyrin agar plates, indicating their tributyrin-hydrolyzing activity (Fig. 5). For that, both recombinant *Yarrowia* cells and supernatants collected after 72-h cultivation were used to assess the hydrolysis due to the cell wall-displayed Lip2 in the first case but also due to the lipases secreted in the medium. In the second case, the activity is owing to native secreted lipases but also likely due to leaks of *promoter*-driven *YlPIR1-LIP2* gene expression, resulting in non-cell wall-anchored Lip2. Since the supernatant from the wild-type strain did not form any visible halo, we conclude that the non-cell wall-anchored Lip2 is primarily responsible for the hydrolytic activity of the recombinant strains. Although agar-based methods do not provide precise and accurate quantitation, the results are consistent with the outcome of the pNPP assay, i.e., the dual, hybrid, and *EXP1* promoter systems outperformed the *H3*. The weakness of the pH3 compared to the pEXP1 was also evident at 48-, 72-, and 96-h plates, where the supernatant formed a bigger halo, indicating a higher leakage. While this method cannot distinguish between the best-performing strains, it provides useful insights regarding leakage and inefficient anchoring.

Large-scale production of biocatalytic biomass

To identify factors that can be fine-tuned to simultaneously maximize biomass production and Lip2 activity, and to elucidate their interplay, large-scale yeast cultivation was performed using a 3-L benchtop bioreactor. For that, the strain bearing the hybrid promoter UAS1B8-TMAL(250)-YlPIR1-LIP2 IntC_2 was chosen, since it had the highest pNPP transesterification activity (Fig. 4B). For bench scale biomass propagation, two different strategies were followed: (i) high agitation speed to maintain optimal oxygen levels in the medium, ensuring robust biomass formation, and (ii) low agitation speed to enhance Lip2 anchoring, preserve the functional conformation of the protein, and mitigate excessive shear and oxygen stress.

For benchtop scale experiments, cells were cultivated in flasks containing liquid YPG medium at 30 °C with shaking at 150 rpm. Bioreactor scale-up was performed using a 3-L Minifors 2 bioreactor (Infors HT, Bottmingen, Basel, Switzerland) equipped with control units for pH,

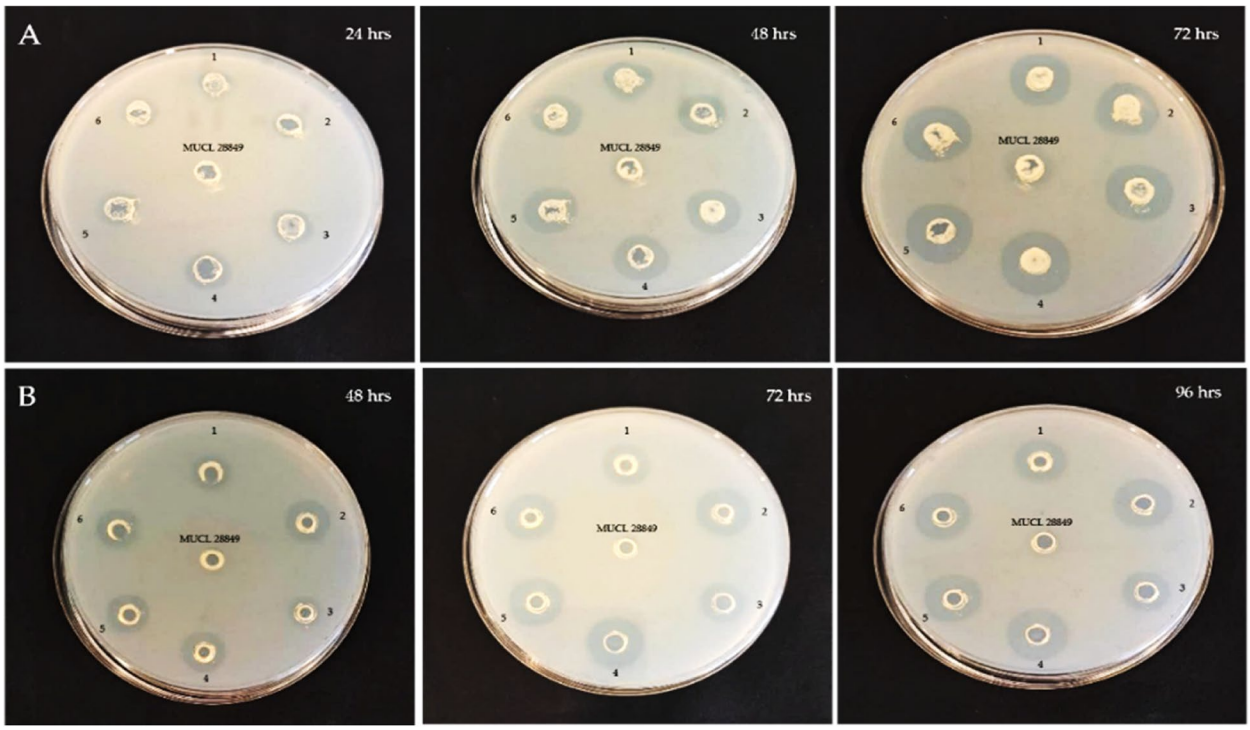

Fig. 5 Screening of recombinant *Y. lipolytica* strains on tributyrin agar plates. **A** Cultures of recombinant *Y. lipolytica* strains grown on YPG agar at 24, 48, and 72 h. **B** Supernatants of recombinant *Y. lipolytica* cultures after 72-h incubation at 30 °C and 150 rpm. Strains are arranged in a clockwise direction: (*center*) WT MUCL 28849 as control; 1) EXP1-YlPIR1-LIP2 IntE_4. 2) H3-YlPIR1-LIP2 IntF_3. 3) EXP1-YlPIR1-LIP2 IntF_3. 4) EXP1-YlPIR1-LIP2 IntE_4/EXP1-YlPIR1-LIP2 IntF_3. 5) EXP1-YlPIR1-LIP2 IntE_4/H3-YlPIR1-LIP2 IntF_3. 6) UAS1B8-TMAL(250)-YlPIR1-LIP2 IntC_2

temperature, oxygen, and agitation speed. The bioreactor, containing 1 L of YPG medium, was inoculated with a starting OD_{600nm} of 0.5 from YPG precultures, and cells were cultivated at 28 °C. Dissolved oxygen was measured with an electrode and maintained at 40% using a PID control system which enabled automatic adjustments to agitation speed (ranging from 150–300 rpm for low to 500–800 rpm for high settings) and air sparging (1–1.5 vvm). The initial pH (6.5–6.8) was allowed to freely vary during the batch phase. Cell growth was monitored by measuring OD_{600nm}.

Under conditions of high agitation (cascade 500–800 rpm) (Fig. 6A), the highest biomass formation was achieved after approximately 13 h of cultivation, when cells entered the stationary phase, reaching an OD_{600nm} above 100. Exponential growth occurred in two phases: from 2 to 8 h with a growth rate of 0.46 $h^{-1}$and from 8 to 13 h with a reduced rate of 0.33 h^{-1}. This pattern can be attributed to the fact that dissolved oxygen is in excess at the beginning but at some point (in this case 8 h) dramatically drops, however at levels that can still sustain exponential yeast growth. Once glycerol was depleted, cells entered the stationary phase. During this period, pH dropped below 5.0 after 8 h and reached its lowest value of 4.2 at 12 h, likely due to the secretion of metabolites such as citric or acetic acid. However, *Y. lipolytica* thrives in a broad pH range, including acidic conditions as in this case, where growth was not impaired. To assess the activity of the produced biomass, samples were withdrawn at 8, 10, and 12 h, lyophilized, and tested for pNPP transesterification with butanol. Maximum lipase activity, approximately 4.5 ± 1.4 Ug_{CDW}^{-1}, was determined after 12 h of cultivation, corresponding to the end of the exponential phase.

On the other hand, when a low agitation cascade (150–300 rpm) was employed (Fig. 6B), the growth rate decreased to 0.36 h^{-1}. Cells entered early stationary phase already between 8–10 h of cultivation, reaching a maximum OD_{600nm} of 33 after 72 h, nearly threefold lower and requiring a longer cultivation period compared to high agitation conditions. Although low agitation supported cell growth, this condition was suboptimal for high-density batches due to the aerobic nature of the yeast. Strict exponential growth took place the first 8–10 h, while oxygen level remained adequate. Once the pO_2 dropped below 3–4%, the cells transitioned into the stationary phase. Under low agitation, glycerol remained available in the medium, even after 72 h of cultivation, reaching a yield of biomass on carbon source of 1.7, compared to 4.9 under high agitation. Similarly, pH decreased but at a slower rate and dropped below 5 after 48 h. With maximum agitation (300 rpm) and aeration (1.5 vvm), biomass formation continued but at a slow rate. The residual glycerol at the end of the batch indicates that oxygen availability, rather than glycerol, was the limiting factor for biomass formation. Interestingly, mild agitation did not result in increased biomass production as expected; however, cells cultivated under these conditions exhibited nearly fourfold higher catalytic activity, observed during the stationary phase (Fig. 6B) in contrast to high agitation conditions, where activity peaked during the exponential phase.

In this study, stirring speed controlled the efficiency of oxygen delivery to the culture medium in the bioreactor. It is well established that increasing the stirring speed reduces the size of gas bubbles, thereby increasing their total surface area. This more finely distributed gas leads to more efficiently oxygen transfer from the gas to the liquid phase and therefore improved oxygenation. Constant stirring not only reduces the size of the gas bubbles that arise in the culture vessel—it also distributes nutrients to the cells required for their growth. However, in cases of sensitive cell cultures, such in this study, where the cell surface-displayed enzymes have to retain their functional conformation and concomitantly their activity, it seems that high agitation can induce oxidative damage, leading to their denaturation [50, 51]. Therefore, even though the gassing rate was the same under both conditions, high agitation speed favored biomass formation but at the expense of the catalytic performance, while low agitation speed had the opposite effect. Apparently, high stirring speed facilitated effective aeration (O_2 transfer and dispersion) and nutrient mass transfer, leading to high biomass titers, however, with low biocatalytic activity. Conversely, low stirring speed, despite providing suboptimal aeration that limited growth (low growth rate and biomass titer), preserved the biocatalytic activity, which increased as cells entered the stationary phase.

Synthesis of biodiesel via methyl esterification of olive oil using *Yarrowia* cell surface-displayed Lip2

The catalytic performance of the yeast biomass was evaluated in methanolysis reactions using olive oil as substrate for the production of biodiesel. For that, the recombinant strain UAS1B8-TMAL(250)-YlPIR1-LIP2 IntC_2 was cultivated in a batch bioreactor under low agitation conditions (150–300 rpm), and after 72 h, biomass was harvested and lyophilized. Key parameters that affect the production of FAMEs were investigated, such as water content, stepwise methanol addition, and the presence of silica gel in the reaction medium. The molar ratio of olive oil to methanol and biocatalyst loading were kept constant at 1:3 [52] and 20% w/w_{oil}, respectively. Regarding water content, biodiesel production was catalyzed using 0%, 5%, 10%, 15%, and 20% v/w_{oil} at 40 °C, 200 rpm, and samples were analyzed with GC-FID. Even

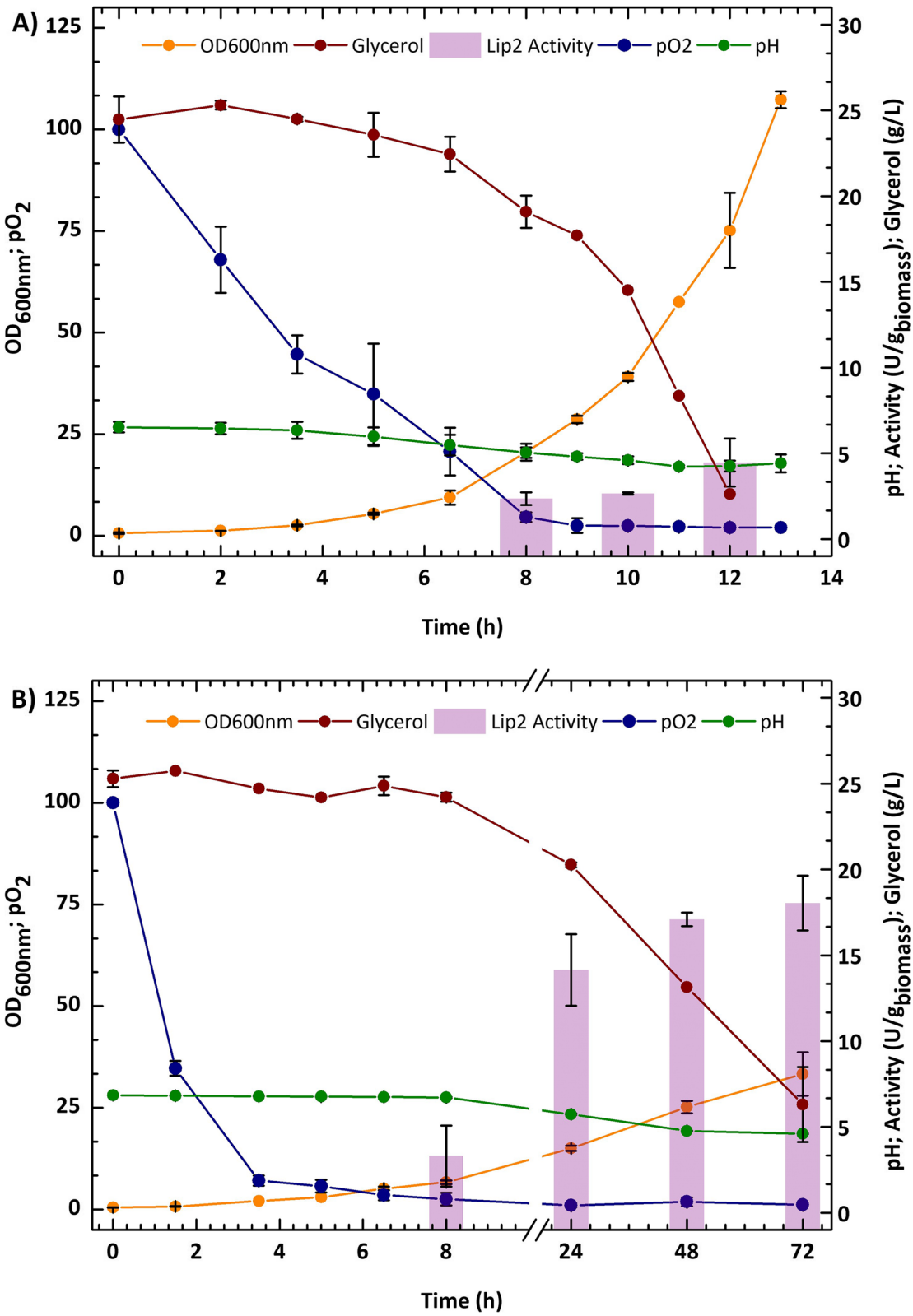

Fig. 6 Monitoring of OD_{600nm}, glycerol concentration, Lip2 activity, dissolved oxygen (pO_2), and pH in bioreactor fermentations of recombinant *Y. lipolytica* UAS1B8-TMAL(250)-YlPIR1-LIP2 IntC_2. The pO_2 control system enabled automatic adjustment of agitation under two conditions: **A** High-speed agitation (500–800 rpm) and **B** low-speed agitation (150–300 rpm). Data points represent the mean values of three biological replicates ($n = 3$), with standard deviations shown as error bars

though the presence of water promotes soap formation through hydrolysis of oil triglycerides, thereby reducing both biodiesel yield and quality, water strongly influences lipase activity which is high at an optimum water content [53, 54]. Lipase activity is enhanced at oil–water interfaces, where interfacial activation occurs, a phenomenon that involves the transition of lipase from their inactive (closed) form to their active (open) form, exposing hydrophobic regions of the protein to the interface [55]. When 20% v/w_{oil} water was added, a 13-fold increase in conversion yield was achieved (Supplementary Fig. S1). Lipase inactivation by methanol during biodiesel production is an additional hurdle that is often overcome by stepwise addition [56]. In this study, methanol was added in three stages: at the beginning of the reaction and after 5 and 24 h (40 °C, 200 rpm). This approach increased conversion yield to 55.2%, compared to 12.9% when methanol was added in a single step (0 h). The addition of silica gel to the reaction mixture is also found to enhance biodiesel yield by facilitating acyl migration and subsequent methyl esters formation [57–60]. When silica gel (6% w/w_{oil}) was incorporated, conversion yield further increased to 71.4% (Fig. 7A). According to Spanou et al., microbial strains displaying lipases on their cell surface have been reported to achieve biodiesel yields ranging from approximately 31 to over 95%. These systems typically involve *P. pastoris* or *S. cerevisiae* cells with various lipases (e.g., CALB, TLL, ROL) displayed on their cell surface [54]. In a similar study on the cell surface display of *Y. lipolytica* lipase Lip2 using the cell wall protein YlPir1, a whole-cell biocatalyst was developed for biodiesel synthesis recycling. When applied to two consecutive cycles of soybean oil methanolysis (200 rpm, 37 °C), the biocatalyst achieved methyl ester yields of 84.1% and 71.0% after 33 and 45 h of reaction, respectively [21]. Although direct yield comparisons are challenging due to variations in biocatalytic systems, the whole-cell biocatalyst presented here appears to be a promising candidate for biodiesel production.

Finally, biocatalyst reusability was assessed under conditions that lead to the highest conversion yields, i.e., three-step methanol addition in the absence and presence of silica gel. Samples were withdrawn 24 h after the last methanol addition, and each reaction cycle (40 °C, 200 rpm) lasted 7 days. The biomass was reused for three consecutive cycles, with fresh substrates added at the start of each cycle. According to the results, and taking into account the long duration of each cycle (i.e., FAMES analysis at 48 h and additional 120-h incubation), UAS1B8-TMAL(250)-YlPIR1-LIP2 IntC_2 biomass showed a notable operational stability, with a decline in its activity from the first to the second cycle, of approximately 46% and 51% in the absence and presence of silica gel, respectively. By the third cycle, the biomass had lost 82% and 76% of its activity under the respective conditions. Studies have demonstrated that lipases can be reused for multiple cycles; however, their activity tends to decline over time due to continuous operation and deactivation by short-chain alcohols and glycerol [56, 61, 61, 62]. The stability and reusability of cell surface-displayed lipases may be lower than those of commercially available immobilized enzymes. Immobilization generally provides stronger, more permanent

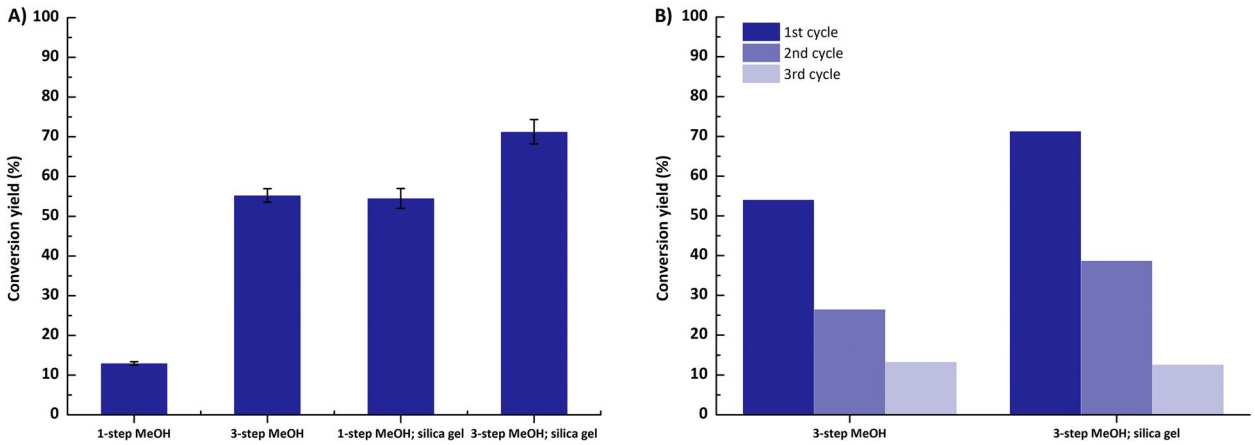

Fig. 7 **A** Effect of stepwise methanol addition and silica gel in the reaction mixture on % conversion yield. Reactions were catalyzed by 20% w/w_{oil} UAS1B8-TMAL(250)-YlPIR1-LIP2 IntC_2 biomass, which was grown in a bioreactor under low agitation conditions (150–300 rpm), harvested after 72-h cultivation, and lyophilized. Reaction conditions: 3:1 molar ratio of methanol to olive oil, 40 °C, and 200 rpm for 48 h. Methyl heptadecanoate in n-hexane (10 mg/mL) was used as the internal standard for quantification, according to the EN 14103 standard method [44]. Data points represent the mean values of two biological replicates ($n = 2$), with standard deviations shown as error bars. **B** Biocatalyst reusability under conditions of stepwise methanol addition with and without silica gel. The reaction conditions were as described above, with each cycle lasting 7 days

attachment to a support matrix (e.g., beads or resins), which shields the enzyme from external factors and helps maintain its structure and functional conformation. In contrast, cell surface-displayed lipases are directly exposed to the surrounding environment, making them more susceptible to degradation or inactivation under harsh conditions. Prolonged exposure to high or even moderate temperatures can cause denaturation, thereby reducing enzyme stability. Additionally, protein misfolding during the expression and display process may compromise stability and catalytic activity, rendering the enzyme more prone to denaturation or degradation [5]. Unlike commercially available immobilized lipases, which are typically optimized for both activity and stability to ensure consistent performance across a range of conditions, operational factors, such as high substrate concentrations or mechanical agitation, can weaken the interactions between enzymes and the cell surface, leading to enzyme detachment and gradual loss of activity. In some cell surface-display systems, the enzyme–substrate interactions may also be less efficient due to constraints imposed by the cell wall or membrane, further diminishing activity and stability over time [63]. Immobilized lipases, on the other hand, often interact more freely with substrates, and the immobilization matrix can be engineered to minimize inhibitory effects. Clearly, enzyme stability is a complex issue that requires balancing multiple factors to ensure long-term functionality in industrial applications, such as biodiesel production. To address these challenges, strategies such as optimizing reaction conditions (e.g., temperature, agitation, and solvent) [54, 64], using stabilizing agents [15, 65, 66], improving cell surface engineering [5, 8, 13], and developing synergetic co-displayed enzymes (combi lipases) or cosolvents can be effective [9, 67].

Effect of carbon source on the activity of the *Yarrowia* cell surface-displayed Lip2

It is well known that the type of carbon source used in the culture medium influences both lipase production and secretion [68–71]. For example, it was found that for *Y. lipolytica* CBS6303 wild-type strain, the production of extracellular lipase Lip2 was stimulated by the presence of long-chain fatty acid, whereas in glucose-containing media extracellular lipase activity was detected at relatively low levels and only after glucose depletion [72]. Similar findings were observed when triglycerides (olive oil, sunflower oil, tributyrin) and fatty acids (oleic acid) were added to a glucose containing basal medium of *Y. lipolytica* CECT 1240 [73]. In this work, to analyze the impact of the carbon source on lipase production and display efficiency, the activity of cell surface-displayed Lip2 was determined using biomass of the UAS1B8-TMAL(250)-YlPIR1-LIP2 IntC_2 strain grown on YPG medium supplemented with 5% v/v olive oil, waste cooking olive oil, or molasses. As shown in Fig. 8, supplementation with any of the above substrates induced lipase synthesis and/or display efficiency, as measured by the pNPP assay using 72-h biomass as the catalyst.The activity increased by 53% and 57% for olive oil and molasses,

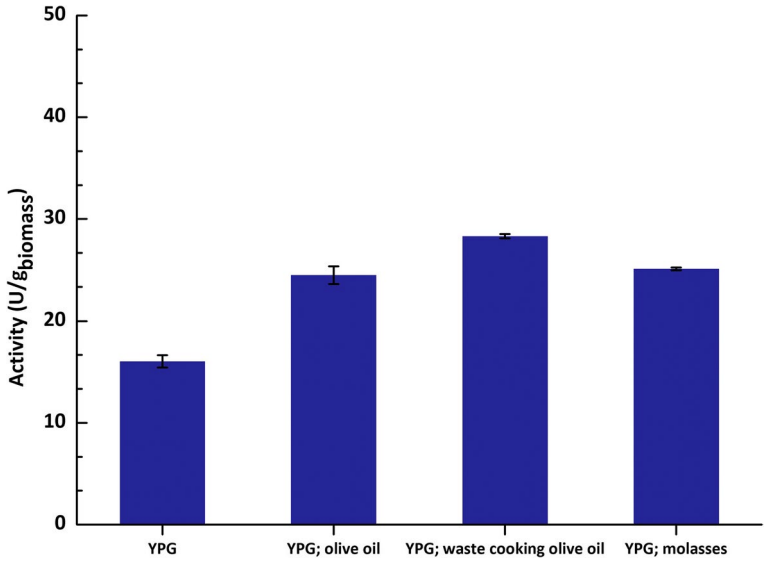

Fig. 8 Effect of carbon source on the enzymatic activity of the UAS1B8-TMAL(250)-YlPIR1-LIP2 IntC_2 biomass. Biomass was harvested after 72 h of cultivation in flasks (30 °C, 150 rpm) and lyophilized. One unit of biomass activity was defined as 1 µmol of p-nitrophenol released per minute at 40 °C using 10-mM pNPP and 1-M butanol in hexane as substrates. Data points represent the mean values of two biological replicates ($n = 2$), with standard deviations shown as error bars

respectively, while in the case of waste cooking olive oil by 76%, likely due to the higher content of free fatty acids (FFAs) and breakdown products generated during cooking that are more readily metabolized and induce lipase production [74–77].

Conclusions

The display of enzymes on the surface of yeast cells is an advantageous strategy for the construction of stable, highly effective, and low-cost whole-cell biocatalysts. With the aid of powerful synthetic biology tools, tailor-made biocatalysts can be designed, built, and optimized to have specific characteristics, such as improved catalytic performance or tolerance to process-specific parameters. For efficient cell surface engineering, it is crucial to select a suitable gene expression system for recombinant protein production, an appropriate anchor protein to achieve high display efficiency, and an easy-to-handle microbial host.

Compared to other systems commonly used for biodiesel production, such as immobilized enzymes or enzyme combinations (combi systems), the stability and efficiency of cell surface-displayed lipases can be further compromised by factors like environmental stress on host cells (e.g., high agitation), enzyme detachment, gradual loss from the cell surface, improper folding, exposure to harsh conditions leading to denaturation, and dependence on cell integrity. However, yeast cells offer a cost-effective solution by serving as both enzyme carriers and biocatalysts, eliminating the need for expensive and time-consuming enzyme isolation, purification, and recovery steps. Yeast is relatively easy and inexpensive to cultivate on a large scale, making it a sustainable and low-cost alternative to traditional enzyme recovery methods. Furthermore, the ease of cell separation and recovery further reduces operational expenses, facilitating continuous operation and automation. Although yeast surface display systems show significant promise, initial optimization and scale-up may incur costs related to genetic engineering of yeast strains, culture optimization, and bioreactor design. Nevertheless, these initial expenses are generally offset over time by the reduced need for enzyme purification and the reusability of the system.

In the present study, taking advantage of the high protein secretion capacity of *Y. lipolytica* and the availability of purposeful genetic tools, we demonstrated a convenient method for preparing stable whole-cell catalysts displaying active Lip2 lipase on the cell surface that can be used directly after cultivation and harvest for biodiesel production. Under optimal conditions (methanol-oil ratio 3:1, biocatalyst loading 20% w/w_{oil}, water content 20% v/w_{oil}, three-step methanol addition, silica gel 6% w/w_{oil}), the engineered strain enabled efficient biodiesel production from olive oil methanolysis, achieving a yield of 71.4% after 48 h, rendering the strain a promising whole-cell catalyst for producing biodiesel from vegetable and waste oils. Biomass harvesting after strain cultivation in a lab scale bioreactor revealed that even though high agitation supports high cell density cultures, it can also promote a deleterious effect on the biocatalytic activity of the displayed enzyme due to protein denaturation. However, a fed-batch system, using the dissolved oxygen concentration as substrate feed indicator, can be designed to allow control over the culture growth while maintained at levels that do not trigger the inactivation of the cell surface-displayed enzyme. The whole-cell biocatalyst can be cost-effectively produced at large scale using waste cooking oil as carbon source, offering great potential for industrial biotechnological applications.

Abbreviations

OD	Optical density
EGFP	Enhanced green fluorescent protein
EXP	Export protein
H3	Histone 3
DO	Dissolved oxygen
FAME	Fatty acid methyl esters
GC-FID	Gas chromatography flame ionization detector
HPLC	High-pressure liquid chromatography
μ	Microbial growth rate (h^{-1})

Supplementary Information

The online version contains supplementary material available at https://doi.org/10.1186/s44314-025-00021-w.

Additional file 1. Table S1. List of plasmids used in this study. Table S2. List of primers used in this study. Table S3. List of primers used in this study for verification of successful excision of antibiotic resistance gene *NAT*. Figure S1. GC-FID chromatograms obtained from the analysis of reaction mixtures after 7 d of reaction at 40 °C, 200 rpm, 3:1 ratio of methanol:olive oil, and catalysed by UAS1B8-TMAL(250)-YlPIR1-LIP2 IntC_2 biomass grown in bioreactor under low agitation conditions (150-300 rpm), harvested after 72 h of cultivation, and lyophilized. Upper panel: Water content of 0% v/w (black), 5% v/w (pink), 10% v/w (purple), 15% v/w (brown), 20% v/w (green). Lower panel: Biocatalyst loading of 0% w/w (black), 1% w/w (pink), 2.5% w/w (purple), 5% w/w (brown), 10% w/w (green), 20% w/w (dark blue).

Acknowledgements

The authors would like to thank Irina Borodina for generously providing access to the EasyClone YALI-Integrative vector set, Agata Smogorzewska for providing the LentiCRISPRv2-*mCherry* plasmid, Doug Golenbock for providing the pcDNA3-*EGFP* plasmid, and Prof. Emmanuel Panteris for providing access and helping with CLSM in School of Biology, Faculty of Sciences, Aristotle University of Thessaloniki.

Authors' contributions

E.P. performed part of the experimental work (synthetic biology, flow cytometry, microscopy) and participated in data interpretation, M.O. performed part of the experimental work (yeast physiology, enzymatic assays, large-scale cultivations, biodiesel production) and participated in data interpretation, E.T. participated in funding acquisition, study conception and design, supervision, and prepared the manuscript draft. A.M.M. participated in funding acquisition, study conception and design, supervision, and reviewed the final manuscript.

Funding
This research has been co-financed by the European Regional Development Fund of the European Union and Greek national funds through the EPAnEk-NSRF 2014–2020-Operational Programme Competitiveness, Entrepreneurship & Innovation, under the call RESEARCH–CREATE–INNOVATE (project code: T2EDK-00573).

Data availability
No datasets were generated or analysed during the current study.

Ethics approval and consent to participate
Not applicable.

Consent for publication
All authors approved the final manuscript and the submission to the journal.

Competing interests
The authors declare no competing interests.

Received: 19 December 2024 Accepted: 10 March 2025
Published online: 04 April 2025

References

1. Shibasaki S, Maeda H, Ueda M. Molecular display technology using yeast–arming technology. Anal sciences : the international journal of the Japan Society for Analytical Chemistry. 2009;25(1):41–9. https://doi.org/10.2116/ANALSCI.25.41.
2. Lee SY, Choi JH, Xu Z. Microbial cell-surface display. Trends Biotechnol. 2003;21(1):45–52. https://doi.org/10.1016/S0167-7799(02)00006-9.
3. Zhang C, Chen H, Zhu Y, Zhang Y, Li X, Wang F. Saccharomyces cerevisiae cell surface display technology: strategies for improvement and applications. Frontiers in Bioengineering and Biotechnology. 2022;10(December):1–15. https://doi.org/10.3389/fbioe.2022.1056804.
4. Han L, Zhao Y, Cui S, Liang B. Redesigning of microbial cell surface and its application to whole-cell biocatalysis and biosensors. Appl Biochem Biotechnol. 2018;185(2):396–418. https://doi.org/10.1007/S12010-017-2662-6.
5. Teymennet-Ramírez KV, Martínez-Morales F, Trejo-Hernández MR. Yeast surface display system: strategies for improvement and biotechnological applications. Front Bioeng Biotechnol. 2022;9. https://doi.org/10.3389/FBIOE.2021.794742.
6. Ueda M, Tanaka A. Genetic immobilization of proteins on the yeast cell surface. Biotechnol Adv. 2000;18(2):121–40. https://doi.org/10.1016/S0734-9750(00)00031-8.
7. Guirimand G, et al. Cell-surface display technology and metabolic engineering of: Saccharomyces cerevisiae for enhancing xylitol production from woody biomass. Green Chem. 2019;21(7):1795–808. https://doi.org/10.1039/c8gc03864c.
8. Smith MR, Khera E, Wen F. Engineering novel and improved biocatalysts by cell surface display. Ind Eng Chem Res. 2015;54(16):4021–32. https://doi.org/10.1021/ie504071f.
9. Yan Y, Xu L, Dai M. A synergetic whole-cell biocatalyst for biodiesel production. RSC Adv. 2012;2(15):6170–3. https://doi.org/10.1039/C2RA20974H.
10. Iyyappan J, Jayamuthunagai J, Bharathiraja B, Saravanaraj A, Praveen Kumar R, Balraj S. Production of biodiesel from Caulerpa racemosa oil using recombinant Pichia pastoris whole cell biocatalyst with double displayed over expression of Candida antartica lipase. Bioresource technology. 2022;363:127893. https://doi.org/10.1016/J.BIORTECH.2022.127893.
11. Urbar-Ulloa J, et al. Cell surface display of proteins on filamentous fungi. Appl Microbiol Biotechnol. 2019;103(17):6949–72. https://doi.org/10.1007/s00253-019-10026-7.
12. Dong C, et al. Engineering Pichia pastoris with surface-display minicellulosomes for carboxymethyl cellulose hydrolysis and ethanol production. Biotechnol Biofuels. 2020;13(1). https://doi.org/10.1186/S13068-020-01749-1.
13. Liu Y, et al. Development of a: Pichia pastoris whole-cell biocatalyst with overexpression of mutant lipase i PCLG47I from Penicillium cyclopium for biodiesel production. RSC Adv. 2018;8(46):26161–8. https://doi.org/10.1039/c8ra04462g.
14. Huang D, Han S, Han Z, Lin Y. Biodiesel production catalyzed by Rhizomucor miehei lipase-displaying Pichia pastoris whole cells in an isooctane system. Biochem Eng J. 2012;63:10–4. https://doi.org/10.1016/J.BEJ.2010.08.009.
15. Sena RO, et al. Application of Rhizomucor miehei lipase-displaying Pichia pastoris whole cell for biodiesel production using agro-industrial residuals as substrate. Int J Biol Macromol. 2021;189:734–43. https://doi.org/10.1016/J.IJBIOMAC.2021.08.173.
16. Han ZL, Han SY, Zheng SP, Lin Y. Enhancing thermostability of a Rhizomucor miehei lipase by engineering a disulfide bond and displaying on the yeast cell surface. Appl Microbiol Biotechnol. 2009;85(1):117–26. https://doi.org/10.1007/S00253-009-2067-8/FIGURES/6.
17. Raoufi Z, Mousavi Gargari SL. Biodiesel production from microalgae oil by lipase from Pseudomonas aeruginosa displayed on yeast cell surface. Biochemical Engineering Journal. 2018;140:1–8. https://doi.org/10.1016/J.BEJ.2018.09.008.
18. Zhao N, Xu Y, Wang K, Zheng S. Synthesis of isomalto-oligosaccharides by Pichia pastoris displaying the Aspergillus niger α-glucosidase. J Agric Food Chem. 2017;65(43):9468–74. https://doi.org/10.1021/acs.jafc.7b04140.
19. Yang S, Lv X, Wang X, Wang J, Wang R, Wang T. Cell-surface displayed expression of trehalose synthase from Pseudomonas putida ATCC 47054 in Pichia pastoris using Pir1P as an anchor protein. Frontiers in Microbiology. 2017;8(DEC):1–9. https://doi.org/10.3389/fmicb.2017.02583.
20. Jiang ZB, Song HT, Gupta N, Ma LX, Wu ZB. Cell surface display of functionally active lipases from Yarrowia lipolytica in Pichia pastoris. Protein Expr Purif. 2007;56(1):35–9. https://doi.org/10.1016/j.pep.2007.07.003.
21. Yuzbasheva EY, et al. Cell surface display of Yarrowia lipolytica Lipase Lip2p using the cell wall protein YlPir1p, its characterization, and application as a whole-cell biocatalyst. Appl Biochem Biotechnol. 2015;175(8):3888–900. https://doi.org/10.1007/s12010-015-1557-7.
22. An J, et al. An alternative approach to synthesizing galactooligosaccharides by cell-surface display of β-galactosidase on Yarrowia lipolytica. J Agric Food Chem. 2016;64(19):3819–27. https://doi.org/10.1021/acs.jafc.5b06138.
23. Wang H, et al. Genetical surface display of silicatein on Yarrowia lipolytica confers living and renewable biosilica-yeast hybrid materials. ACS Omega. 2020;5(13):7555–66. https://doi.org/10.1021/acsomega.0c00393.
24. Bulani SI, Moleleki L, Albertyn J, Moleleki N. Development of a novel rDNA based plasmid for enhanced cell surface display on Yarrowia lipolytica. AMB Express. 2012;2(1):1–8. https://doi.org/10.1186/2191-0855-2-27.
25. Yang X, Jiang Z, Song H, Jiang S, Madzak C, Ma L. Cell-surface display of the active mannanase in Yarrowia lipolytica with a novel surface-display system. Biotechnol Appl Biochem. 2009;54(3):171–6. https://doi.org/10.1042/ba20090222.
26. Yuzbasheva EY, Yuzbashev TV, Gvilava IT, Sineoky SP. Protein display on the Yarrowia lipolytica yeast cell surface using the cell wall protein YlPir1. Appl Biochem Microbiol. 2012;48(7):650–5. https://doi.org/10.1134/S0003683812070058.
27. Wang JM, et al. Construction of arming Yarrowia lipolytica surface-displaying soybean seed coat peroxidase for use as whole-cell biocatalyst. Enzyme and Microbial Technology. 2020;135(December 2019):109498. https://doi.org/10.1016/j.enzmictec.2019.109498.
28. Georgiadis I, et al. Identification and construction of strong promoters in Yarrowia lipolytica suitable for glycerol-based bioprocesses. Microorganisms. 2023;11(5):pp. https://doi.org/10.3390/microorganisms11051152.
29. Deng J, et al. A synthetic promoter system for well-controlled protein expression with different carbon sources in Saccharomyces cerevisiae. Microb Cell Fact. 2021;20(1):1–10. https://doi.org/10.1186/s12934-021-01691-3.
30. Inokuma K, Bamba T, Ishii J, Ito Y, Hasunuma T, Kondo A. Enhanced cell-surface display and secretory production of cellulolytic enzymes with Saccharomyces cerevisiae Sed1 signal peptide. Biotechnol Bioeng. 2016;113(11):2358–66. https://doi.org/10.1002/bit.26008.
31. Yang X, Tang H, Song M, Shen Y, Hou J, Bao X. Development of novel surface display platforms for anchoring heterologous proteins in

Saccharomyces cerevisiae. Microb Cell Fact. 2019;18(1):1–10. https://doi.org/10.1186/s12934-019-1133-x.
32. Aza P, Molpeceres G, de Salas F, Camarero S. Design of an improved universal signal peptide based on the a-factor mating secretion signal for enzyme production in yeast. Cell Mol Life Sci. 2021;78(7):3691–707. https://doi.org/10.1007/s00018-021-03793-y.
33. Phienluphon A, et al. Identification and evaluation of novel anchoring proteins for cell surface display on Saccharomyces cerevisiae. Appl Microbiol Biotechnol. 2019;103(7):3085–97. https://doi.org/10.1007/s00253-019-09667-5.
34. Inokuma K, Kurono H, den Haan R, van Zyl WH, Hasunuma T, Kondo A. Novel strategy for anchorage position control of GPI-attached proteins in the yeast cell wall using different GPI-anchoring domains. Metabolic Engineering. 2020;57(November 2019):110–7. https://doi.org/10.1016/j.ymben.2019.11.004.
35. Tang H, et al. Engineering vesicle trafficking improves the extracellular activity and surface display efficiency of cellulases in Saccharomyces cerevisiae. Biotechnol Biofuels. 2017;10(1):1–13. https://doi.org/10.1186/s13068-017-0738-8.
36. Huang M, Wang G, Qin J, Petranovic D, Nielsen J. Engineering the protein secretory pathway of Saccharomyces cerevisiae enables improved protein production. Proc Natl Acad Sci USA. 2018;115(47):E11025–32. https://doi.org/10.1073/pnas.1809921115.
37. Besada-Lombana PB, Da Silva NA. Engineering the early secretory pathway for increased protein secretion in Saccharomyces cerevisiae. Metab Eng. 2019;55(June):142–51. https://doi.org/10.1016/j.ymben.2019.06.010.
38. Wang W, Blenner MA. Engineering heterologous enzyme secretion in Yarrowia lipolytica. Microb Cell Fact. 2022;21(1):1–10. https://doi.org/10.1186/s12934-022-01863-9.
39. Akil E, et al. Accessing regio-and typo-selectivity of Yarrowia lipolytica lipase in its free form and immobilized onto magnetic nanoparticles. Biochem Eng J. 2016;109:101–11. https://doi.org/10.1016/j.bej.2015.12.019.
40. Chen DC, Yang BC, Kuo TT. One-step transformation of yeast in stationary phase. Curr Genet. 1992;21(1):83–4. https://doi.org/10.1007/BF00318659.
41. Holkenbrink C, et al. EasyCloneYALI: CRISPR/Cas9-based synthetic toolbox for engineering of the yeast Yarrowia lipolytica. Biotechnol J. 2018;13(9). https://doi.org/10.1002/biot.201700543.
42. Carrazco-Palafox J, Rivera-Chavira BE, Ramírez-Baca N, Manzanares-Papayanopoulos LI, Nevárez-Moorillón GV. Improved method for qualitative screening of lipolytic bacterial strains. MethodsX. 2018;5:68–74. https://doi.org/10.1016/j.mex.2018.01.004.
43. Fu X, Zheng J, Ying X, Yan H, Wang Z. Investigation of lipozyme TL IM-catalyzed transesterification using ultraviolet spectrophotometric assay. Cuihua Xuebao/Chinese Journal of Catalysis. 2014;35(4):553–9. https://doi.org/10.1016/s1872-2067(14)60053-x.
44. European Standard (2003) Fat and Oil Derivatives-Fatty Acid Methyl Esters (FAME)-Determination of Ester and Linolenic Acid Methyl Ester Contents. EN 14103: 2003.
45. He S, Zhang Z, Lu W. Natural promoters and promoter engineering strategies for metabolic regulation in Saccharomyces cerevisiae. Journal of Industrial Microbiology and Biotechnology. 2023;50(1):kuac029. https://doi.org/10.1093/jimb/kuac029.
46. Yuzbasheva EY, Yuzbashev TV, Laptev IA, Konstantinova TK, Sineoky SP. Efficient cell surface display of Lip2 lipase using C-domains of glycosylphosphatidylinositol-anchored cell wall proteins of Yarrowia lipolytica. Appl Microbiol Biotechnol. 2011;91(3):645–54. https://doi.org/10.1007/s00253-011-3265-8.
47. Moon HY, Van TL, Cheon SA, Choo J, Kim JY, Kang HA. Cell-surface expression of Aspergillus saitoi-derived functional α-1,2-mannosidase on Yarrowia lipolytica for glycan remodeling. J Microbiol. 2013;51(4):506–14. https://doi.org/10.1007/s12275-013-3344-x.
48. Kajiwara K, Aoki W, Ueda M. Evaluation of the yeast surface display system for screening of functional nanobodies. AMB Express. 2020;10(1). https://doi.org/10.1186/s13568-020-00983-y.
49. Liu Y, Zhang R, Lian Z, Wang S, Wright AT. Yeast cell surface display for lipase whole cell catalyst and its applications. J Mol Catal B Enzym. 2014;106:17–25. https://doi.org/10.1016/j.molcatb.2014.04.011.
50. Hawkins CL, Davies MJ. Detection, identification, and quantification of oxidative protein modifications. J Biol Chem. 2019;294(51):19683–708. https://doi.org/10.1074/jbc.REV119.006217.
51. Van Hecke W, et al. Bubble-free oxygenation of a bi-enzymatic system: effect on biocatalyst stability. Biotechnol Bioeng. 2009;102(1):122–31. https://doi.org/10.1002/bit.22042.
52. Srimhan P, Kongnum K, Taweerodjanakarn S, Hongpattarakere T. Selection of lipase producing yeasts for methanol-tolerant biocatalyst as whole cell application for palm-oil transesterification. Enzyme Microb Technol. 2011;48(3):293–8. https://doi.org/10.1016/j.enzmictec.2010.12.004.
53. Atadashi IM, Aroua MK, Aziz ARA, Sulaiman NMN. The effects of water on biodiesel production and refining technologies: a review. Renew Sustain Energy Rev. 2012;16(5):3456–70. https://doi.org/10.1016/j.rser.2012.03.004.
54. Spanou A, Moschona A, Theodosiou E, Patsios SI, Pavlidis IV. Novel concepts for the biocatalytic synthesis of second-generation biodiesel. Front Catal. 2024;4:1360702. https://doi.org/10.3389/fctls.2024.1360702.
55. Reis P, Holmberg K, Watzke H, Leser ME, Miller R. Lipases at interfaces: a review. Adv Coll Interface Sci. 2009;147–148:237–50. https://doi.org/10.1016/j.cis.2008.06.001.
56. Lotti M, Pleiss J, Valero F, Ferrer P. Enzymatic production of biodiesel: strategies to overcome methanol inactivation. Biotechnol J. 2018;13(5). https://doi.org/10.1002/biot.201700155.
57. Du W, Xu Y-Y, Liu D-H, Li Z-B. Study on acyl migration in immobilized lipozyme TL-catalyzed transesterification of soybean oil for biodiesel production. J Mol Catal B Enzym. 2005;37(1):68–71. https://doi.org/10.1016/j.molcatb.2005.09.008.
58. Mazzieri VA, Vera CR, Yori JC. Adsorptive properties of silica gel for biodiesel refining. Energy Fuels. 2008;22(6):4281–4. https://doi.org/10.1021/ef800479z.
59. Lee M, Lee J, Lee D, Cho J, Kim S, Park C. Improvement of enzymatic biodiesel production by controlled substrate feeding using silica gel in solvent free system. Enzyme Microb Technol. 2011;49(4):402–6. https://doi.org/10.1016/j.enzmictec.2011.06.020.
60. Mangas-Sánchez J, Adlercreutz P. Highly efficient enzymatic biodiesel production promoted by particle-induced emulsification. Biotechnol Biofuels. 2015;8(1):58. https://doi.org/10.1186/s13068-015-0247-6.
61. Hwang HT, et al. Lipase-catalyzed process for biodiesel production: protein engineering and lipase production. Biotechnol Bioeng. 2014;111:639–53. https://doi.org/10.1002/bit.25162/abstract.
62. Sankaran R, Show PL, Chang JS. Biodiesel production using immobilized lipase: feasibility and challenges. Biofuels, Bioprod Biorefin. 2016;10(6):896–916. https://doi.org/10.1002/bbb.1719.
63. Li Y, Wang X, Zhou N-Y, Ding J. Yeast surface display technology: mechanisms, applications, and perspectives. Biotechnol Adv. 2024;76: 108422. https://doi.org/10.1016/j.biotechadv.2024.108422.
64. Sandaka BP, Kumar J, Melo JS. Mitigation of methanol inactivation of lipases by reaction medium engineering with glycine betaine for enzymatic biodiesel synthesis. Fuel. 2022;313: 122637. https://doi.org/10.1016/j.fuel.2021.122637.
65. Xu R, et al. A betaine-modified whole-cell biocatalyst with surface display of Thermomyces lanuginosus lipase for biodiesel production from Jatropha curcas oil. Ind Crops Prod. 2023;205: 117479. https://doi.org/10.1016/j.indcrop.2023.117479.
66. Hama S, Yoshida A, Nakashima K, Noda H, Fukuda H, Kondo A. Surfactant-modified yeast whole-cell biocatalyst displaying lipase on cell surface for enzymatic production of structured lipids in organic media. Appl Microbiol Biotechnol. 2010;87(2):537–43. https://doi.org/10.1007/s00253-010-2519-1.
67. Jin Z, Han SY, Zhang L, Zheng SP, Wang Y, Lin Y. Combined utilization of lipase-displaying Pichia pastoris whole-cell biocatalysts to improve biodiesel production in co-solvent media. Biores Technol. 2013;130:102–9. https://doi.org/10.1016/J.BIORTECH.2012.12.020.
68. Fickers P, Nicaud JM, Gaillardin C, Destain J, Thonart P. Carbon and nitrogen sources modulate lipase production in the yeast Yarrowia lipolytica. J Appl Microbiol. 2004;96(4):742–9. https://doi.org/10.1111/j.1365-2672.2004.02190.x.
69. Fickers P, Ongena M, Destain J, Weekers F, Thonart P. Production and down-stream processing of an extracellular lipase from the yeast Yarrowia lipolytica. Enzyme Microb Technol. 2006;38(6):756–9. https://doi.org/10.1016/j.enzmictec.2005.08.005.
70. Fickers P, Destain J, Thonart P. Improvement of Yarrowia lipolytica lipase production by fed-batch fermentation. J Basic Microbiol. 2009;49(2):212–5. https://doi.org/10.1002/jobm.200800186.

71. Fickers P, Marty A, Nicaud JM. The lipases from Yarrowia lipolytica: genetics, production, regulation, biochemical characterization and biotechnological applications. Biotechnol Adv. 2011;29(6):632–44. https://doi.org/10.1016/j.biotechadv.2011.04.005.
72. Fickers P, Nicaud JM, Destain J, Thonart P. Overproduction of lipase by Yarrowia lipolytica mutants. Appl Microbiol Biotechnol. 2003;63(2):136–42. https://doi.org/10.1007/s00253-003-1342-3.
73. Domínguez A, Deive FJ, Sanromán MA, Longo MA. Effect of lipids and surfactants on extracellular lipase production by Yarrowia lipolytica. J Chem Technol Biotechnol. 2003;78(11):1166–70. https://doi.org/10.1002/jctb.922.
74. Domínguez A, Deive FJ, Angeles Sanromán M, Longo MA. Biodegradation and utilization of waste cooking oil by Yarrowia lipolytica CECT 1240. European Journal of Lipid Science and Technology. 2010;112(11):1200–8. https://doi.org/10.1002/ejlt.201000049.
75. Colacicco M, Ciliberti C, Agrimi G, Biundo A, Pisano I. Towards the physiological understanding of Yarrowia lipolytica growth and lipase production using waste cooking oils. Energies. 2022;15(14):pp. https://doi.org/10.3390/en15145217.
76. Yan J, et al. Engineering Yarrowia lipolytica to simultaneously produce lipase and single cell protein from agro-industrial wastes for feed. Sci Rep. 2018;8(1):758. https://doi.org/10.1038/s41598-018-19238-9.
77. Lopes M, Miranda SM, Alves JM, Pereira AS, Belo I. Waste cooking oils as feedstock for lipase and lipid-rich biomass production. Eur J Lipid Sci Technol. 2019;121(1): 1800188. https://doi.org/10.1002/ejlt.201800188.

Publisher's Note